Distinct Kinetic Signatures of Photodesorption from Metal Nanoparticles

Arik Beck[1,2,*], Michael J. Gordon[1], Phillip Christopher[1,*]

[1] Department of Chemical Engineering, University of California Santa Barbara, Santa Barbara, CA 93106, USA

[2] Institute for Chemical Technology and Polymer Chemistry, Karlsruhe Institute of Technology KIT, 76131 Karlsruhe, Germany

* Correspondence to: arik.beck@kit.edu, pchristoper@ucsb.edu

Abstract

Visible photon fluxes can influence the rate and selectivity of heterogeneously catalyzed reactions on metal nanoparticle surfaces. Models describing the influence of photon fluxes have typically introduced photon flux dependent apparent thermal kinetic parameters (reaction orders, activation energies, binding energies, etc.). This has involved empirical fitting of reaction rate data, making mechanistic interpretations of the influence of photon fluxes on elementary step rates challenging and is inconsistent with fundamental descriptions of photochemistry on metal surfaces developed from surface science studies. Using the CO adsorption-desorption quasi-equilibrium reaction on Pt/Al_2O_3 catalysts as a model system, we measured steady-state adsorbed CO (CO*) coverages under isothermal and isobaric (1 mbar CO) conditions as a function of temperature (473 – 573 K) and of 440 nm photon flux (0.1-5.2 x 10^3 $\#_{hv}$ Pt site^{-1} s^{-1}) using in-situ IR spectroscopy. Steady state CO* coverage on Pt was strongly photon flux dependent with increasing photon flux causing decreasing coverage, consistent with photons driving CO* desorption rates faster than thermal CO* desorption rates. However, photon flux dependent CO* coverages were essentially temperature independent, inconsistent with models that describe photon effects using perturbations to apparent thermal kinetic parameters. Instead, 120 steady state CO* coverages as a function of temperature and photon flux are quantitatively described by a kinetic model in which the overall desorption rate is a summation of independent thermal and photon-induced CO* desorption rates. Site-resolved analysis reveals distinct kinetic parameters for the photon driven desorption of CO* from well-coordinated, under-coordinated, and highly under-coordinated Pt sites, with temperature-dependent apparent quantum efficiencies (AQE) consistent with temperature dependence of vibrational quanta distribution of adsorbed CO. The rigorous kinetic rate laws for independent photon and thermal driven pathways allow for predictive modeling of the influence of photon fluxes on the rates of CO* desorption under catalytic conditions. Further, the analysis provides evidence that steady state continuous wave photon fluxes can drive desorption/adsorption reactions on metal surfaces out of thermal equilibrium, reconciling surface science observations of molecular photodesorption with applied catalysis. The work establishes a general kinetic framework to be considered for photon-driven processes on metals, and defines catalyst, reaction, and photon flux characteristic design principles for breaking Sabatier limitations.

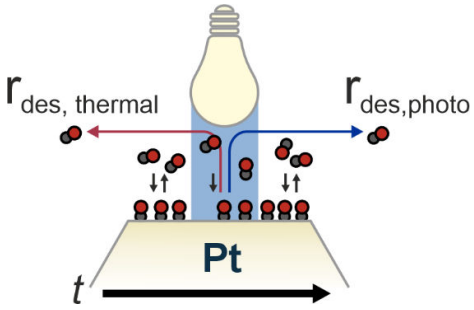

Introduction

Visible photon fluxes can impact the performance of heterogeneously catalyzed reactions on metal nanoparticle surfaces, leading to enhancements in reaction rates,[1–3] product selectivity,[4–6] and catalyst stability[7] compared to pure thermally driven reactions. Further, photon-driven reactions on metal surfaces may proceed through distinct reaction mechanisms.[8,9] The unique behavior of visible photon-driven catalysis on metal surfaces is generally attributed to the participation of electronically or vibrationally non-equilibrated species in kinetically relevant elementary steps.[10–13] Driving kinetically relevant elementary steps in catalytic cycles out of thermal equilibrium has been proposed as one approach to breakdown Sabatier limitations to reaction rates or selectivity.[14] Realizing the potential of photon-driven elementary steps for targeted catalytic chemistry requires insights into how photon fluxes influence reaction microkinetics (the rates of elementary steps) to enable predictions of performance as a function of reaction conditions, catalyst composition, and photon flux characteristics. Accurate kinetic models may further elucidate underlying photochemical mechanisms, including how active site and elementary step identity influence photochemical efficiency. Emerging concepts such as "programmable catalysis",[15,16] which predicts transient modulation of catalyst states (driving systems out of temporal quasi-equilibrium) to surpass Sabatier limitations, likewise depend on fundamental models describing how photon illumination alters microkinetics.[17]

Previous efforts to model experimental data on the influence of photon fluxes on catalytic reactivity have introduced modified apparent thermal kinetic parameters. For example, photon flux dependent changes of the binding energy of adsorbates[16], apparent and elementary step activation energies[3,16,18–21], and reaction orders[3,20,21] have been proposed. While empirical models have often accounted for photon flux effects by modifying apparent thermal kinetic parameters, this strategy can lead to misinterpretation of the underlying mechanisms governing elementary reaction steps. Because most systems studied involve complex, multi-component catalysts and reactions comprising multiple elementary steps (i.e., adsorption, surface reactions, desorption), it is challenging to pinpoint which elementary step rates are affected by photons and at which types of active sites.[3] Further, kinetic parameters such as reaction orders and apparent activation energies can be influenced by variations in temperature, making it challenging to differentiate influences of photochemistry and photon induced heating.[22,23]

In contrast and sometimes detached from the more recent developments in photon driven chemistry over metal nanoparticles, surface science studies made substantial progress in understanding the influence of short laser pulses (ns-fs) on elementary reaction step kinetics and mechanisms on single crystals.[24–27] Temporally resolved measurements of vibrational, rotational, and kinetic states of molecules desorbing from metal surfaces in response to short photon pulses provided direct evidence of non-equilibrium energy distributions in desorbing and reacting molecules resulting from energy exchange in electronically excited states.[24,28] However, powder catalyst samples composed of multiple materials with multi-faceted nanoparticles are expected to behave differently than single crystal

samples due to the existence of distinct active sites and distinct optical properties (coupling of photon fluxes to potential energy surfaces).[5,14,29]

In order to cross the divide between application oriented photon driven chemistry on supported metal nanoparticles[1,9,30] and fundamental mechanistic knowledge from surface science on metal single crystals,[24–27] experimental analyses of the kinetic behavior of "simple" reaction networks are needed. Ideally this would be achieved by studying the kinetics of elementary reaction steps on supported metal catalysts as a function of photon flux characteristics, reaction conditions and active site characteristics. For example, we recently investigated the influence of visible photon fluxes on the rate of CO* desorption from powdered Al_2O_3-supported Pt and Pd nanoparticle catalysts during temperate programmed desorption (TPD) measurements, where adsorbed CO coverage was measured via Diffuse Reflectance Infrared Fourier Transformed Spectroscopy (DRIFTS).[31] Theoretical analyses suggested that the resonant absorption of visible photons (440 nm) with electronic transitions localized at the Pt-CO surface carbonyl complex[32] resulted in enhanced desorption rates of CO from Pt compared to the thermal energy provided. The resonant absorption is the consequence of a transition from hybridized Pt-CO orbitals with predominantly metal character into the unoccupied portion of the antibonding Pt-CO orbitals of mostly molecule character. The resulting energy transfer weakens the CO-Pt bond facilitating its desorption.[33]

While CO-TPD experiments provided clear evidence of photon-flux enhancement of desorption rates compared to thermal desorption, extracting reliable kinetic parameters from CO-TPD experiments under visible photon fluxes remains challenging. Photon fluxes influenced the "shape" of the relationship between CO coverage and temperature, deviating from first-order behavior. These deviations may be difficult to quantify due to transient temperature variations during the introduction of photon fluxes and uncertainties in surface temperature measurements (this is an inherently non steady state measurement). Additionally, CO* desorption occurring within the bed volume probed by the IR and subsequent re-adsorption onto nearby sites can further complicate the choice of kinetic models.[34] To establish rigorous kinetic models and provide justified kinetic parameter estimations for the influence of photon fluxes on the rate of CO* desorption from supported Pt surfaces, experiments should explicitly address the influence of photothermal heating, temperature transients, and re-adsorption. Further, large and consistent data sets as a function of temperature, photon flux, and CO coverage are needed to develop robust models.

In the present work, we use steady state isobaric and isothermal CO* coverage measurements on Pt/Al_2O_3 powder catalysts as a function of photon flux and catalyst temperature to address limitations of previous experimental analyses. Surprisingly, CO* coverage on the Pt surface as a function of temperature and photon flux could not be effectively modelled by kinetic expressions with photon flux dependent apparent thermal kinetic parameters. Instead, effective modelling required two separate rate expressions for thermal and photodesorption of CO from Pt, where photodesorption rates are comparatively weakly temperature dependent and require description by a non-microscopically reversible rate expression. Rigorous modeling allowed for extraction of site-specific rate constants and apparent quantum efficiencies (AQEs) for CO* photodesorption from Pt as a function of temperature and photon flux. The resulting kinetic models enable accurate predictions of photon-driven rates of elementary steps in catalytic processes and provide strong evidence that the introduction of a photon flux drives the CO adsorption-desorption process away from thermal quasi-equilibrium. Our finding challenges the typical approach used by the field to model the influence of photon fluxes on catalytic rates and further suggests that photon driven reactions can be envisioned as photolytic processes that are out of thermal equilibrium and occur separately from thermally driven reactions.

Results and Discussion

Steady-state measurements of photon driven CO* desorption from Pt

To elucidate the underlying mechanism and kinetic description of visible photon flux induced CO* desorption from Pt nanoparticles, a well-characterized Pt/γ-Al_2O_3 catalyst was used (synthesized via incipient-wetness impregnation).[31] Sequential O_2 and H_2 treatments at 573 K were used *in-situ* to remove adventitious carbon species and reduce oxidized Pt nanoparticles into a metallic state. After the H_2 reductive pretreatment, the Pt nanoparticles were 1.2 ± 1.1 nm in diameter on volume normalized basis.[31] CO absorbed on Pt surfaces (CO*) gives rise to strong infrared active vibrational modes, which were measured by DRIFTS and used to follow CO* coverage as a function of temperature and photon flux.[35] 440 nm photon fluxes (0.05-2.35 W/cm^2; 0.1 – 5.2 x 10^{18} $\#_{h\nu}$ cm^{-2} s^{-1}; 0.1-5.2 x 10^3 $\#_{h\nu}$ Pt site^{-1} s^{-1}) were introduced via a continuous wave laser fed through a light guide into the *in-situ* DRIFTS cell depicted in Figure 1a. The units of $\#_{h\nu}$ Pt site^{-1} s^{-1} are calculated by normalizing photon flux per cm^2 by the areal density of metal sites at the surface of an FCC metal (1.5 * 10^{15} sites cm^{-2}) to estimate the maximum rate of photon absorption per Pt site if the absorption cross section were identical to the physical cross section. To account for photon-induced heating, a thermocouple was placed directly in the catalyst bed, which we have shown accurately reflects steady-state temperature increases for this material.[23,31]

To avoid transient changes in the reaction environment (e.g., temperature, re-adsorption rates, etc.) during CO* coverage measurements, we measured steady-state CO* coverage under isothermal and isobaric conditions (p(CO) = 1 mbar) as a function of 440 nm photon flux. We chose 440 nm photons because our previous work demonstrated that this is the resonant photon energy for driving electronic transitions localized at the Pt-CO bond and subsequent CO* desorption from Pt nanoparticle surfaces.[5,16,31] Isobaric experiments allow the surface to be modeled as quasi-equilibrated at a steady-state temperature and photon flux, where CO coverage reflects the "quasi-equilibrium" between adsorption and desorption rates. This experimental design avoids transient temperature and re-adsorption rates that are inherent in TPD measurements and complicate kinetic parameter estimation. The idea of "quasi-equilibrium" in this system in the context of photochemical steps is discussed further below.

The experimental protocol is depicted in Figure 1b (see also Supporting Figures S1-3). The DRIFT spectrum of CO* was measured in the dark at a given temperature and then the sample was illuminated at a constant photon flux for 5 min, after which the temperature returned to the setpoint (as measured by the thermocouple in the bed and controlled by current provided to the cell heaters) and the IR spectrum reached steady-state (Supporting Figure S4). Subsequently, the photon source was turned off, and after 5 min, the spectrum was measured in the dark again. The two dark measurements were used to probe whether the spectrum of CO* and, consequently the Pt surface structure, were irreversibly changed by exposure to the photon flux. The experiment was automated and photon fluxes were introduced in randomized order at each temperature. Figure 1c depicts selected spectra at 573 K in 1000 ppm CO under illumination at increasing photon fluxes and corresponding dark spectra after photon exposure. The steady-state measurements under CO atmosphere showed a photon flux-dependent decrease in the area and shape of the CO* IR spectra, demonstrating that increased photon fluxes cause decreased steady state intensity of the CO* IR band. In the context of the previously observed promotion in the rate of CO* desorption from Pt under 440 nm photons,[16,31] we interpret the decrease in the peak area as a change of CO* coverage on the Pt nanoparticle surfaces. Importantly, the spectra of CO* collected under dark conditions remained similar in shape and intensity before and after each photon exposure period and across the 50-hour experiment, indicating that Pt did not undergo substantial changes over the course of the experiment (Supporting Figure S5).

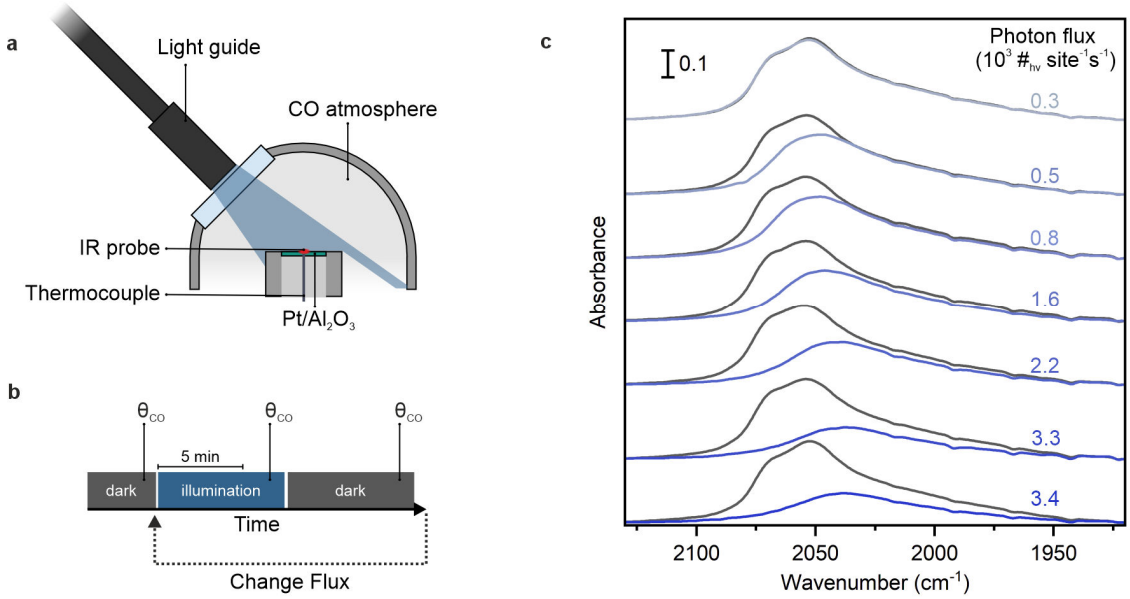

Figure 1: (a) Experimental setup for *in-situ* CO-DRIFTS under visible photon illumination. (b) Protocol for measurements of isothermal and isobaric CO* steady state coverage under photon illumination and in the dark. The θ_{CO} mark indicates when IR spectra were collected during the experiment to determine the steady state CO* coverage on Pt. For all experiments, 1000 ppm CO with a balance of Ar was used at 1 bar and temperature was varied between 473 – 573K. (c) Steady state CO-DRIFT spectra collected at 573 K under different photon fluxes (blue) and the corresponding spectra collected in the dark (grey) acquired in between the different illumination sequences. The inset notes the photon flux for each spectrum collected under illumination.

The experiment was performed for 30 different photon fluxes at 4 temperatures (473, 533, 553, and 573 K) for a total of 360 steady state CO* measurements (120 under photon flux and 240 in the dark). In 1 mbar of CO and the explored temperatures, the spectrum collected in the dark was consistent and corresponded to "saturation" coverage of the Pt surface (Supporting Figure S5). Figure 2a shows the steady state CO* band area, A, for all temperatures normalized to the value in the dark $A_{0,\,473\,K}$ at 473 K, providing a first approximation of CO* coverage, θ_{CO}, as a function of photon flux. Flux is expressed in photons per Pt site per second, as described above, which can be envisioned as the photon flux per area of a metal site if the absorption cross section were identical to the physical cross section. In our experiments, the divergent beam of the 4 W laser produced an estimated areal photon flux per site on the millisecond timescale at the surface of the catalyst bed. Across all explored temperatures, the relationships between θ_{CO} and photon flux were surprisingly similar. The absence of a temperature dependence indicates that a kinetic description of photon-induced CO* desorption requires moving beyond conventional thermocatalytic models where photon flux dependent CO* binding energies (activation energies for desorption) would exhibit temperature dependent desorption rates at a constant photon flux. This finding also provides incontrovertible evidence that photon induced heating of the sample is not the cause of the decrease in CO* band intensity for the same reasoning.

To provide a site-specific analysis of photon induced CO* desorption, we decomposed the CO* band and assigned the three components to particular CO* adsorption sites (example given in Figure 2b). The decomposition differentiates between three features at 2070 cm^{-1}, associated with CO chemisorbed on well-coordinated Pt sites (WC, terraces), 2050 cm^{-1} related to CO on under-coordinated sites (UC, step edges), and a feature summing together multiple features < 2030 cm^{-1} assigned to CO on "highly under-coordinated" sites (HUC, kink and point defect sites).[35,36] We note that despite potential changes in the position of bands associated with CO bound to each type

of site in the presence of strong dipole-dipole coupling, this assignment has been proven as we discuss further below.[35] Using site specific extinction coefficients,[35] we approximated the fractional coverage of CO* normalized to surface saturation on the different adsorption sites, X_i, as a function of photon flux. X_i is defined as:

$$X_i = \frac{A_i/\varepsilon_i}{\sum_{i=1}^{3} A_{i,0}/\varepsilon_i} \quad (1)$$

with i = 1 – 3 corresponding to WC, UC, and HUC sites and specific extinction coefficients of each species given as $\varepsilon_{WC} = 1$ and $\varepsilon_{UC} = \varepsilon_{HUC} = 2.7$.[35] This approximation assumes of a linear relationship between peak area and CO* coverage.

It is important to carefully consider the assumption of linear dependence of IR intensity and CO* coverage on a certain adsorption site. This assumption is considered reasonable as small nanoparticles limit dipole-dipole coupling between adsorbed CO molecules due to high radius of curvature.[35] Alternatively, the influence of vibrational coupling on IR intensity on the surface of curved nanoparticles, even without band shifts that are commonly associated with dipole coupling, has previously been associated with "collective modes" on the nanoparticles; i.e., all CO vibrating in phase on a spherical particle would generate no net dipole and have no IR intensity.[37] However, the influence of collective modes on the resulting vibrational spectrum occurs for particle models that are symmetric, which is clearly not consistent with irregularly shaped supported nanoparticles in our materials where no "collective" dipole for all adsorbed species will develop as there is no centrosymmetric axis. Our data show no band shifts outside the high-coverage envelope as coverage decreases and the integrated IR intensity, as a function of temperature, fits well to Temkin models. All together, our data and understanding suggests minimal influence of vibrational coupling on the relationship between CO* coverage and IR intensity under our explored conditions. However, we do acknowledge this as an intrinsic limitation of CO IR spectroscopy – also with respect to peak assignment to specific Pt coordination – and recommend future studies using mixed-isotope ^{13}CO experiments and coverage-dependent extinction coefficient measurements.[38]

Figure 2c shows the photon flux dependent CO* coverage change for all sites at 473 K. Similar to the $A/A_{0,\,473\,K}$ analysis for the entire spectrum (Figure 2a), after peak fitting, all temperatures result in nearly the same flux dependent change in CO* coverage (Supporting Figure S6). At 473 K, when the photon flux is increased from 0 to 3.2 x 10^3 $\#_{hv}$ $site^{-1}$ s^{-1}, the fraction of CO* (normalized to saturation coverage) drops from 0.44 to 0.05 on WC sites, from 0.18 to 0.03 on UC sites, and from 0.4 to 0.2 on HUC sites. This result shows that photon-induced CO* desorption occurs with site-specific rates, where CO* desorption from WC Pt sites appears to be the most efficient.

Based on a comparison of CO-TPD data under dark conditions (Supporting Figure S7) to our isothermal and isobaric photodesorption experiments, we observed no significant changes in spectral shape at a given coverage. This suggests that under the tested conditions CO* diffusion across the Pt surface is fast. As CO* coverage decreases – either due to increased photon-induced desorption at higher flux or thermal desorption at elevated temperatures – adsorbed CO* remains mobile and redistributes among available sites, preferentially occupying the more strongly binding, under-coordinated Pt sites.[39,40]

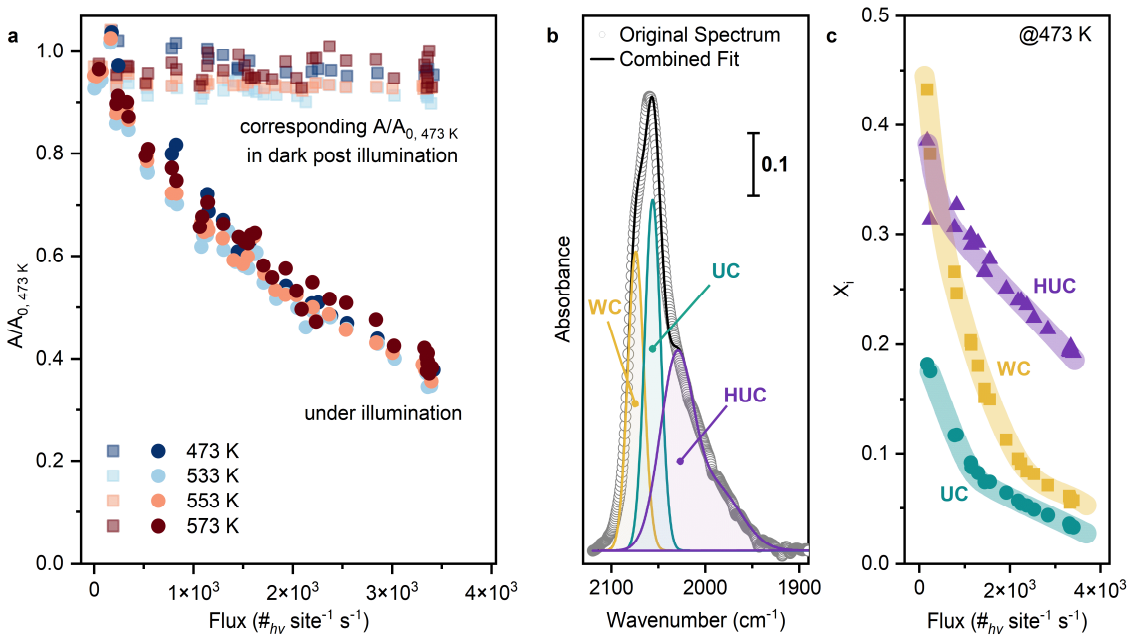

Figure 2: Spectral analysis and apparent temperature independence of photon-induced CO* desorption from Pt. (a) Change of $A/A_{0,\,473\,K}$ (area of the spectrum under photon illumination normalized by the area in the dark at 473 K) as a function of 440 nm photon flux at 473, 533, 553, and 573 K under 0.1 mbar CO (total pressure 1 bar, balanced with Ar). Also shown is the corresponding $A/A_{0,\,473\,K}$ without illumination (dark) that was measured directly after the illumination (squares). The constant nature of $A/A_{0,\,473\,K}$ in the dark of ~1 indicated that photon illumination is not irreversibly altering the Pt structure. (b) Exemplary peak fitting of the CO-Pt stretching region assuming three major contributions from CO* on well-coordinated (WC), under-coordinated (UC) and highly under-coordinated (HUC) Pt surface sites. (c) Fraction of specific site coverage of CO* at 473 K as a function of 440 nm photon flux normalized to saturation coverage.

Kinetic model development for photon induced desorption

One of the most striking observations from our study is that CO* coverage remains nearly unchanged across temperatures from 473 to 573 K at the same photon flux. This behavior is unexpected within models that rely on empirically fitting photon flux-dependent apparent kinetic parameters such as binding or activation energies. Combined with the isothermal and isobaric steady-state conditions of our experiments, this finding strongly motivates the development of a new kinetic model to describe the rate of CO* desorption mediated by a photon flux.

We consider two elementary steps in the kinetic analysis, CO adsorption and CO* desorption. Surface migration of CO* on Pt is assumed to be substantially fast and not rate-determining in dictating CO* coverage and, thus, is neglected in the present analysis (this assumes that CO* equilibrates between preferred sites on the Pt surface as described above). Due to the steady-state nature of the experiment, the CO* desorption (r_{des}) and CO adsorption (r_{ads}) rates are assumed to be quasi-equilibrated, and thus the CO* coverage is assumed to be time invariant (see further discussion below) during the IR measurements (see Figure 1b):

$$\frac{d\theta_{CO}}{dt} = 0 = r_{ads} - r_{des} \quad (2).$$

Based on kinetic gas theory, we assume that adsorption is purely thermally driven (we are not aware of processes where photons could influence adsorption rates, as gas phase CO does not absorb visible photons) and thus the rate of adsorption is defined as:

$$r_{ads} = \frac{S(1-\theta)*p_{CO}}{\sqrt{2\pi*m_{CO}*k_B*T}} * e^{-E_{ads}/RT} \quad (3),$$

where S is the sticking coefficient of CO, m_{CO} is the mass of CO, k_B is the Boltzmann constant, E_{ads} is the energy barrier for adsorption (discussed more below), and R is the universal gas constant. For the rate of thermal CO* desorption, we consider the Temkin model assuming a linear dependence of the energy barrier for desorption, E_{des}, on CO* coverage:[41]

$$r_{des} = \nu * e^{-[(1-\theta)*E_{des,\theta=0}+\theta*E_{des,\theta=1}]/RT} * \theta * C_{surf,max} \quad (4),$$

with the desorption barrier at 0 coverage defined as $E_{des,\theta=0}$ and at full coverage as $E_{des,\theta=1}$, the attempt frequency ν, and the saturation CO surface concentration on a Pt as $C_{surf,max}$. During data fitting and parameter estimation, S was restrained to be between 0.8 and 1 following surface science reports from molecular beam experiments.[42] We acknowledge that the sticking coefficient of CO is coverage, structure, and temperature dependent, yet to reduce the number of fitting parameters, we fixed this value.[42] Based on CO-TPD (Supporting Figure S8) and CO temperature-programmed isobar measurements (Supporting Figure S9) in the dark (no photon flux), values for the thermal kinetic parameters were determined to be $E_{des,\theta=0}$ = 156 ± 1 kJ mol^{-1}, $E_{des,\theta=1}$ = 139 ± 1 kJ mol^{-1} and E_{ads} = 32 ± 1 kJ mol^{-1}. The fitting is described in the SI, where uncertainties are calculated based on 95% confidence intervals including Monte Carlo simulation-based noise addition to account for 5% estimated instrumental uncertainty. These values were used to describe r_{ads} and r_{des} under dark conditions.

The reported thermal CO* desorption energies (E_{des}) represent site-averaged values. Using equation (1) and peak fitting obtained in the dark, we estimate that ~77% of the spectral area arises from UC and HUC sites (which is consistent with the small average diameter of the particles), making the obtained values representative of these dominant environments. The extracted $E_{des,\theta=1}$ of 139 kJ mol^{-1} closely matches calculated CO* desorption barrier of 143 kJ mol^{-1} on 6-fold coordinated Pt edge sites,[43] and further, the coverage-dependent range is consistent with reports of CO on Pt(111) (118 kJ mol^{-1} at saturation to 138 kJ mol^{-1} at low coverage).[42] For Pt step sites on Pt(112), literature reports show an additional stabilization of ~33 kJ mol^{-1} compared to Pt(111),[39,40] again consistent with our powder catalyst results. Importantly, our combined fitting of the thermal TPD and isobar experiments coverage yields a nonzero adsorption barrier (E_{ads} = 32 kJ mol^{-1}). While E_{ads} is often assumed negligible, this barrier is likely associated with adsorbate rearrangement required on CO* crowded surfaces to adopt additional CO adsorption events. We hypothesize that CO adsorption on crowded surfaces likely involves lateral diffusion of adsorbates and local Pt reconstruction, both previously reported to exhibit barriers of 23 – 80 kJ mol^{-1}, consistent with the extracted E_{ads}.[40,44] Taken together, the close correspondence between our extracted thermal kinetic parameters and established surface-science benchmarks lends confidence to the fitting procedure and kinetic model describing the adsorption-desorption quasi-equilibrium in the dark.

We next evaluated several kinetic models to describe CO* coverage under photon fluxes within the quasi-equilibrium framework. As a starting point, we adopted the common literature approach in which apparent thermal kinetic parameters (E_{des}) are modified by the photon flux. In this model (equation 5), CO* coverage was calculated from r_{ads} while allowing r_{des} to vary with photon flux by expressing $E_{des,\theta=1}$ as a linear function of flux J, and the resulting fits were compared to the experimental flux- and temperature-dependent CO* coverage (Supporting Figure S10),

$$E_{des,\theta=1} = f(flux) = E_{des,\theta=1,dark} - J * \Delta E_{bind,photo} \quad (5).$$

Here, the constant coefficient, $\Delta E_{bind,photo}$, is assumed to linearly decrease the effective desorption barrier with increasing photon flux, J. Conceptually, $\Delta E_{bind,photo}$, suggests that photons provide vibrational energy into the CO

molecule but that the reaction is still predominantly driven by the background thermal bath of the system. This model predicts sigmoidal shapes of CO* coverage as a function of temperature, with strong temperature dependence of the photochemical contribution, i.e., much weaker photon effects at 473 K than at 573 K. Neither the predicted shape nor the temperature scaling match the experimental data. Extending the model to let $\Delta E_{bind,photo}$ also affect $E_{des,\theta = 0}$ (Supporting Figure S11) or both $E_{des,\theta = 1}$ and $E_{des,\theta = 0}$ (Supporting Figure S12), a modified Temkin model likewise fails to reproduce the observed behavior. We therefore conclude that photon illumination does not act by decreasing E_{bind}, and alternative kinetic models must be considered.

In contrast to the prevailing picture in photochemistry on metals – where photons are assumed to perturb a thermal process – we adopt an alternative view inspired by organometallic photochemistry and previous surface science studies.[45,46] Here, photons drive a distinct photolysis pathway, independent of the thermal channel, and thus require a separate rate description. The relevant time scales underscore this distinction: the average rate of photon-site interactions occur on the order of one per millisecond, while photoexcited states decay within femto- to picoseconds. The reaction following excitation is therefore effectively instantaneous compared to the potential photon absorption rate, consistent with a linear dependence on photon flux.

Next, photon-induced desorption was treated as non-microscopically reversible and therefore only contributing to r_{des} through a distinct rate law from the thermal desorption reaction. Within the catalyst bed probed by the IR measurement, the CW laser with no temporal coherence in the photon flux causes photon absorption at individual Pt-CO complexes to be temporally random and out of phase. This stochastic nature of photon absorption events allows us to model the collective rate of photodesorption within the catalyst bed using macroscopic, probabilistic rate constants. A first-order photodesorption rate is proposed in addition to the thermal desorption term:

$$r_{des} = r_{des,thermal} + r_{des,photo} \qquad (6),$$

with $r_{des,thermal}$ defined by equation (3). As a first test, we assume a temperature-independent photodesorption rate, dependent only on CO* coverage and photon flux, J (Supporting Figure S13):

$$r_{des,photo} = J * \ k'_{AQE} * \theta_{CO} \qquad (7),$$

where the prefactor k'_{AQE} represents the apparent quantum efficiency (AQE) of photodesorption (this is a confluence of the absorption cross section of the Pt-CO complex and internal quantum yield). Supporting Figure S13 shows that, at a fixed temperature, this rate expression captures the flux dependence of CO* coverage well, confirming that a separate rate term is consistent with our experimental observations. However, when fitting the datasets simultaneously across different temperatures, we find that the AQE is temperature-dependent (Figure 3a). For CO* desorption from WC Pt sites, the AQE increases from ~3 % at 473 K to ~15 % at 573 K. This trend indicates that CO* photodesorption AQE exhibits a temperature dependence (although this temperature dependence is independent of photon flux necessitating separation from the thermal desorption rate), motivating the introduction of a temperature dependent term for photodesorption, $E_{A,photo}$, in the photodesorption rate expression (Figure 3b):

$$r_{des,photo} = J * \ k_{AQE} * \theta * e^{-E_{A,photo}/RT} \qquad (8).$$

With appropriate values of $E_{A,photo}$, the model qualitatively and quantitatively reproduces the entire experimental data as a function of photon flux and temperature, including its key nuances (Figure 3b, Table 1).

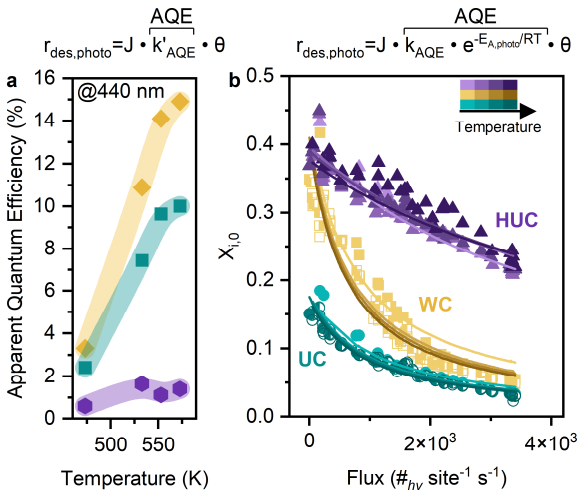

Figure 3: (a) Site-specific AQE as function of temperature (473 – 573 K) predicted using equation (7) to fit the data; a temperature independent photodesorption rate. For this model, AQE is represented by the prefactor k'_{AQE}. (b) Model fit to the site-specific CO* coverage as a function of flux and temperature using the kinetic model based on equation (8) and a temperature-dependent CO* photodesorption rate $r_{des,photo}$. The temperatures measured were 473, 533, 573, and 573 K.

Site	$E_{A,photo}$ [kJ mol^{-1}]	k [CO molecules $\#_{h\nu}^{-1}$ site^{-1}]	R^2 of the overall fit
WC	39 ± 2	$7 \times 10^2 \pm 3 \times 10^2$	0.94
UC	37 ± 1	$3 \times 10^2 \pm 1 \times 10^2$	0.95
HUC	27 ± 2	6 ± 3	0.73

Table 1: Fitting results using equation (8) for $r_{des,photo}$ for CO* desorption from WC, UC, HUC Pt sites. Uncertainties represent 95 % confidence intervals.

CO* photodesorption rates from WC and UC Pt sites exhibit similar exponential temperature dependences ($E_{A,photo} \approx 39 \pm 2$ and 37 ± 1 kJ mol^{-1}), though the prefactor (k_{AQE}) for WC sites is about twice as large as compared to UC. By contrast, HUC sites display both a lower prefactor and a weaker temperature dependence ($E_{A,photo} \approx 27 \pm 2$ kJ mol^{-1}), although the variation in $E_{A,photo}$ is small and likely sensitive to the nature of the fit of the IR spectra. The absolute values of k_{AQE} and $E_{A,photo}$ may deviate due to uncertainties regarding the predetermined thermal parameters (E_{ads}, E_{des}), the Gaussian fitting protocol used for the adsorption site assignment and potential dipole-dipole coupling effects, which may result in a partial non-linearity of the extinction coefficients. Future studies should address these potential effects.

However, the extracted value of 27-39 kJ mol^{-1} for $E_{A,photo}$ allows a physically meaningful interpretation falling in line with previous work on photoexcitation of the Pt-CO bond.[47] In order for photon absorption to result a CO desorption, the energy gain along the potential energy surface (assumed to be vertical motion of CO perpendicular to the surface) has to exceed the binding energy of Pt-CO. These previous theoretical analyses have performed state-to-state scattering calculations for vibrational energy gain in adsorbates on metal surfaces via electronically excited state processes[2,47,48] and found that adsorbates initially in higher vibrational states have an increased probability of gaining energy through photoexcitation. The population of higher vibrational states for Pt-CO is temperature dependent and was calculated to be close to the vibrational energy of bound CO (~ 0.24 eV or 2100 cm^{-1}) to excite CO by a single vibrational quantum.[47] This value is in good agreement with our experimentally observed temperature dependence ($E_{A,photo}$) and provides quantitative confidence in the interpretation of our results.

Thus, it seems likely that the AQE temperature dependence is not inherently a barrier but instead describes how increased population of vibrational states $\nu_i > 0$ (within n = 0) influence the efficiency of the photolysis process. Further, this interpretation also rationalizes the strong site dependency of the photodesorption kinetics. A photo-excitation event must provide sufficient energy to overcome the respective binding energy minus the vibrational state of CO*. This inherently requires more energy gain for stronger binding site (UC and HUC) and thus decreases the likelihood of photodesorption, akin to the original studies of electron stimulated desorption of molecules from W surfaces.[49]

Discussion: Consequences for photon driven reactions on metal surfaces

These experiments demonstrated that the elementary step of photon driven CO* desorption from Pt nanoparticle surfaces cannot be explained merely by adjusting the kinetic parameters describing the thermally driven elementary steps using flux dependent modification. This observation provides direct evidence that the CO adsorption-desorption quasi-equilibrium on Pt nanoparticles is out of thermal equilibrium under the explored CW photon flux. The inability to describe CO* coverage using modified thermal parameters, combined with the temperature-independent flux response, indicates that photon-induced desorption proceeds via a distinct non-thermal reaction pathway that drives the surface chemistry out of thermal equilibrium. The result provides direct evidence that photochemistry on metal nanoparticles using CW sources can control the rates of single elementary steps in catalytic reactions, thus breaking Sabatier limitations.

This finding has fundamental implications for both the applicability and the limitations of photon driven chemistry on metals. The new model aligns well with expected physical phenomena. Given the short lifetime of both the electronic and vibrationally excited states of adsorbates on metal surfaces, it is more plausible that such excitations directly trigger a desorption event or dissipate as thermal energy into the system – analogous to photolysis in organometallic catalysts.[45,46]

Developing a kinetic model for the elementary step of CO* photodesorption enables macroscopic predictions of the influence of photon illumination on the rate of catalytic reactions involving CO* desorption on Pt surfaces. Reactions in which CO* photodesorption could alter catalysis in a rate enhancing manner are, e.g., CO oxidation at low temperatures, where CO* is inhibiting O_2 adsorption;[50] or methanol decomposition in which CO* is the strongly bound product.[16] We want to note that in other catalytic reactions involving CO* as an reactive intermediate, for example NO reduction by CO, photodesorption may be detrimental, as this could decrease the coverage of a reactive intermediate. Furthermore, our work does not provide direct evidence whether photons influence CO* as reactive intermediate transforming into other intermediates (e.g., CO* + O* → CO_2*) with a similar kinetic mechanism. However, it appears likely that other catalytic elementary reaction steps should be described by distinct photon and thermal driven processes. For example, in the case of photon flux promoted NH_3 decomposition on CuRu catalysts, the apparent barrier for the overall reaction decreased from ~120 kJ/mol in the dark to ~30 kJ/mol under optimal illumination conditions. This would be consistent with our proposal of photons driving a rate limiting step (proposed to be 2N* → N_2) in an almost barrierless photolytic step.[3] Consequently, for reactions that follow a similar kinetic framework, our model allows one to systematically identify the reactions, catalysts, and conditions under which photon driven metal catalysis can deliver significant benefits. Hypotheses that were previously built on the assumption of altered binding energies must be reconsidered, and future models should incorporate the proposed kinetic description of how photons influence catalytic kinetics.[15,51,52]

We next consider a catalytic process in which CO* desorption is desired and the rate-limiting step in a catalytic cycle assuming photon fluxes solely influencing this elementary reaction. The proposed kinetic model allows for descriptions of CO* desorption rate in catalytic processes as a summation of thermal desorption and photodesorption. These two processes compete, and photon flux mediated enhancements of overall catalytic rates will only be observed under conditions where photodesorption rates are comparable to, or exceed, the thermal rate of a kinetically relevant step. To illustrate this, Figure 4a shows calculated CO* photodesorption rates from WC, UC, and HUC Pt sites at a photon flux of 1000 photons per site per second (~ 0.5 W/cm^2 of 440 nm photons), alongside the predicted thermal desorption rate of CO*, both derived from our models. Three qualitative regimes can be distinguished. Below 450 K, both photon- and thermal desorption rates of CO* are minimal ($r_{des,thermal,450\ K}$ = 0.0002 molecules CO molecules site^{-1} s^{-1}, $r_{des,photo,450\ K}$ = 13 CO molecules site^{-1} s^{-1} at 1000 $\#_{h\nu}$ site^{-1} s^{-1} with an AQE = 1.3%). A catalytic process requiring CO* desorption as a kinetically relevant step is strongly inhibited at these temperatures. Above 450 K, photodesorption rates become significant (approach 100 CO molecules site^{-1} s^{-1}) owing to its lower activation barrier compared to thermal desorption. Consequently, in the range of 450–700 K, CO* photodesorption rates dominate the overall rates of CO* desorption at the photon fluxes considered in our studies, thus an enhancement in the overall reaction rate should be observed. Beyond 700 K, however, thermal desorption overtakes photodesorption due to its higher activation barrier and dictates the overall rate of CO* desorption. Also worth noting is that as the surface is depopulated of CO*, the rate of photon absorption will decrease because the Pt-CO complex is the primary absorber of 440 nm photons. Related behavior has been reported, for example, the diminished photon-driven rate enhancement for various reactions over Ag catalysts with increasing temperature.[1] Importantly, whether photon mediated elementary steps will contribute significantly to overall reaction kinetics also depends on the site-specific photon mediated reaction kinetics. For example, the AQE for photon mediated CO* desorption is much smaller from HUC sites compared to WC sites; therefore, if the catalytic pathway predominantly involves CO* desorption from HUC sites (rather than WC sites), the overall efficiency of photons will be limited.

One reason why CO* photodesorption rates from Pt nanoparticle surfaces dominates thermal desorption rates over such a wide temperature range in this model is the strong CO–Pt bond and the relatively high AQE. Many catalytic metals – particularly plasmonic metals such as Au, Ag, and Cu – bind intermediates much more weakly. For instance, a binding energy of ~90 kJ mol^{-1} is typical for CO on certain Ag sites.[53] In Figure 4a, the grey line represents the thermal desorption rate of CO* bound with 90 kJ mol^{-1}. Because of this weaker binding, photodesorption remains significantly slower than thermal desorption ($r_{des,thermal,450\ K}$ = 130 molecules CO site^{-1} s^{-1}) even well below 700 K. Figure 4a also depicts the photodesorption rate of CO* from WC sites under a five-fold higher photon flux. This increase in photon flux shifts the onset of photodesorption to lower temperatures, leading once again to a regime where photodesorption dominates, but now at temperatures below 450 K.

Our analysis exemplifies the predictive power of the kinetic model: detailed knowledge of both the photon mediated and thermal kinetics of kinetically relevant elementary steps is essential to assess the relevance of photo-driven processes. Catalytic reactions involving weakly bound intermediates in kinetically relevant steps are unlikely to be strongly manipulated by photon-illumination. This may also explain why, in plasmonic photocatalysis, so-called antenna catalysts dominate applications: the plasmonic materials themselves (Au, Ag, Cu) bind intermediates too weakly, and only the introduction of strong-binding dopants such as Pt, Pd, Ru, or Rh enables substantial photocatalytic enhancement.

Additionally, our analysis underscores the importance of catalyst design in photochemistry by metals. Not only photon-absorption properties but also binding energies must be carefully optimized. Figure 4b illustrates this principle by showing the fraction of the total CO* desorption rate accounted for by photodesorption as a function of temperature. At low temperatures, photodesorption dominates, though the absolute rate is small. Increasing the photon flux by more than an order of magnitude only slightly shifts the temperature at which thermal desorption takes over. In contrast, also shown in Figure 4b, varying the CO* binding energy has a pronounced influence on the temperature range over which photodesorption remains relevant.

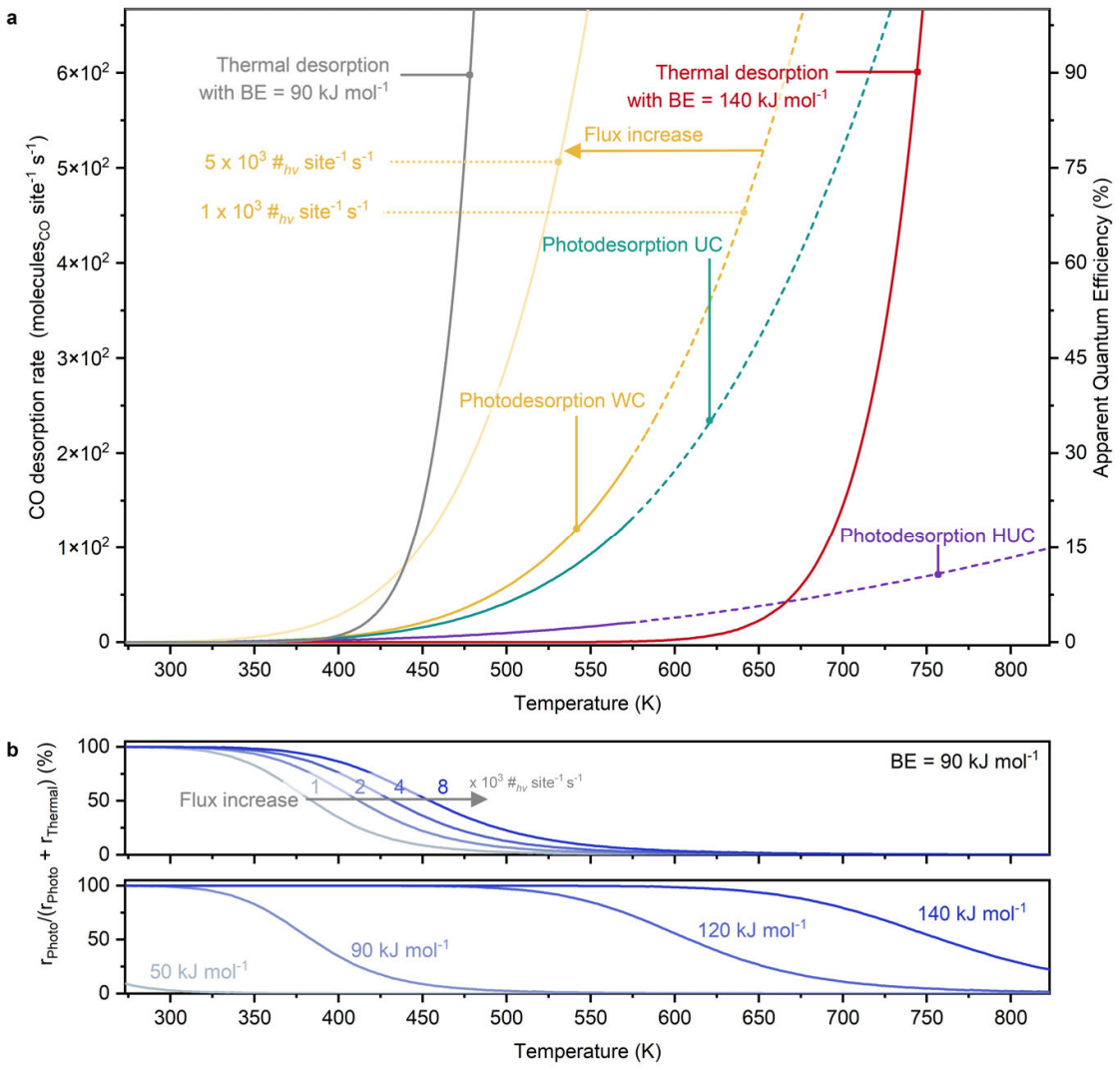

Figure 4: Discussion of the relationship between thermal and photodesorption.(a) Calculated CO* desorption rates from a Pt surface at saturation coverage (θ=1). For thermal desorption, equation (4) is used with two different, exemplary $E_{des,\theta=1}$ (90 and 140 kJ mol^{-1}). For the CO* photodesorption rate from WC, UC, and HUC, equation (8) and a flux of 1 x 10^3 $\#_{h\nu}$ site^{-1} s^{-1} are used. =CO* photodesorption rates from WC are also shown at a flux of 5 x 10^3 $\#_{h\nu}$ site^{-1} s^{-1}. Photodesorption rates beyond the temperature tested in this work is indicated by dashed lines. (b) Shows the relative contribution of CO* photodesorption rate to the overall desorption rate ($r_{photo}/[r_{photo} + r_{thermal}]$) as a function temperature for different photon fluxes (1 – 8 x 10^3 $\#_{h\nu}$ site^{-1} s^{-1}, top panel) and different binding energies (50 – 140 kJ mol^{-1}, bottom panel).

Finally, we address the temperature dependence of CO* photodesorption rates. Because of this temperature dependence, the AQE – defined here as the number of CO molecules desorbed per absorbed photon – rises with increasing temperature. An AQE of unity (100%) corresponds to the desorption of one CO* molecule per photon.

Within the temperature range studied, the AQE for CO* desorption from WC Pt sites is approximately 15% at 573 K and decreases to 6% at 473 K. For CO* bound to UC and HUC Pt sites, the AQE is lower (Figure 4a, right y-axis). At higher temperatures, the AQE formally approaches unity and can even diverge toward infinity. This, however, is unphysical. In practice, several factors limit the AQE: at high desorption rates, surface coverage is depleted, and additional photons cannot induce further desorption due to the lack of adsorbed CO*. Moreover, as desorption accelerates, other processes such as adsorption or mass transport become rate-limiting, thereby constraining the achievable AQE.

Conclusions

In this work, we provide a consistent large set of experimental measurements of CO* coverage on Pt nanoparticle surfaces under isothermal and isobaric conditions as a function of steady state temperature and photon flux. Detailed fitting evidences that previous propositions on photon driven catalytic reactions on metal surfaces likely introduced mechanistically incorrect modifications of apparent thermal kinetic parameters. Our work shows that a summation of two independent CO* desorption rate expressions – one for the photon driven and one for the thermal desorption correctly describes the presented data. The physical interpretation of the model is moreover well in line with surface science studies and organometallic photochemistry. The photon driven process is best described as photolysis, where the photochemical step drives the reacting system out of thermal equilibrium. Therefore, the present work is able to bridge the knowledge of surface science studies to applied photochemistry on metal nanoparticle surfaces. The proposed descriptions of photon driven reaction rate models allow us to predict conditions, catalysts, and reaction that would be altered under photon illumination and further support the notion that photon driven reactions on metal surfaces can surpass Sabatier limitations. Therefore, the work is of fundamental importance for the fields of photon driven and dynamic catalysis, suggesting reconsideration of the mechanistic picture of photochemistry on metal nanoparticle surfaces and paving the way for the design of catalysts and photon flux characteristics to control catalytic processes.

References

(1) Christopher, P.; Xin, H.; Linic, S. Visible-Light-Enhanced Catalytic Oxidation Reactions on Plasmonic Silver Nanostructures. *Nat. Chem.* **2011**, *3* (6), 467–472. https://doi.org/10.1038/nchem.1032.

(2) Christopher, P.; Xin, H.; Marimuthu, A.; Linic, S. Singular Characteristics and Unique Chemical Bond Activation Mechanisms of Photocatalytic Reactions on Plasmonic Nanostructures. *Nat. Mater.* **2012**, *11* (12), 1044–1050. https://doi.org/10.1038/nmat3454.

(3) Zhou, L.; Swearer, D. F.; Zhang, C.; Robatjazi, H.; Zhao, H.; Henderson, L.; Dong, L.; Christopher, P.; Carter, E. A.; Nordlander, P.; Halas, N. J. Quantifying Hot Carrier and Thermal Contributions in Plasmonic Photocatalysis. *Science* **2018**, *362* (6410), 69–72. https://doi.org/10.1126/science.aat6967.

(4) Marimuthu, A.; Zhang, J.; Linic, S. Tuning Selectivity in Propylene Epoxidation by Plasmon Mediated Photo-Switching of Cu Oxidation State. *Science* **2013**, *339* (6127), 1590–1593. https://doi.org/10.1126/science.1231631.

(5) Kale, M. J.; Avanesian, T.; Xin, H.; Yan, J.; Christopher, P. Controlling Catalytic Selectivity on Metal Nanoparticles by Direct Photoexcitation of Adsorbate–Metal Bonds. *Nano Lett.* **2014**, *14* (9), 5405–5412. https://doi.org/10.1021/nl502571b.

(6) Swearer, D. F.; Zhao, H.; Zhou, L.; Zhang, C.; Robatjazi, H.; Martirez, J. M. P.; Krauter, C. M.; Yazdi, S.; McClain, M. J.; Ringe, E.; Carter, E. A.; Nordlander, P.; Halas, N. J. Heterometallic Antenna-Reactor Complexes for Photocatalysis. *Proc. Natl. Acad. Sci. U. S. A.* **2016**, *113* (32), 8916–8920. https://doi.org/10.1073/pnas.1609769113.

(7) Zhou, L.; Martirez, J. M. P.; Finzel, J.; Zhang, C.; Swearer, D. F.; Tian, S.; Robatjazi, H.; Lou, M.; Dong, L.; Henderson, L.; Christopher, P.; Carter, E. A.; Nordlander, P.; Halas, N. J. Light-Driven Methane Dry Reforming with Single Atomic Site Antenna-Reactor Plasmonic Photocatalysts. *Nat. Energy* **2020**, *5* (1), 61–70. https://doi.org/10.1038/s41560-019-0517-9.

(8) Bonn, M.; Funk, S.; Hess, Ch.; Denzler, D. N.; Stampfl, C.; Scheffler, M.; Wolf, M.; Ertl, G. Phonon- Versus Electron-Mediated Desorption and Oxidation of CO on Ru(0001). *Science* **1999**, *285* (5430), 1042–1045. https://doi.org/10.1126/science.285.5430.1042.
(9) Yuan, Y.; Zhou, L.; Robatjazi, H.; Bao, J. L.; Zhou, J.; Bayles, A.; Yuan, L.; Lou, M.; Lou, M.; Khatiwada, S.; Carter, E. A.; Nordlander, P.; Halas, N. J. Earth-Abundant Photocatalyst for H 2 Generation from NH 3 with Light-Emitting Diode Illumination. *Science* **2022**, *378* (6622), 889–893. https://doi.org/10.1126/science.abn5636.
(10) Watanabe, K.; Menzel, D.; Nilius, N.; Freund, H.-J. Photochemistry on Metal Nanoparticles. *Chem. Rev.* **2006**, *106* (10), 4301–4320. https://doi.org/10.1021/cr050167g.
(11) Linic, S.; Christopher, P.; Ingram, D. B. Plasmonic-Metal Nanostructures for Efficient Conversion of Solar to Chemical Energy. *Nat. Mater.* **2011**, *10* (12), 911–921. https://doi.org/10.1038/nmat3151.
(12) Shin, H.-H.; Jeong, J.; Nam, Y.; Lee, K. S.; Yeon, G. J.; Lee, H.; Lee, S. Y.; Park, S.; Park, H.; Lee, J. Y.; Kim, Z. H. Vibrationally Hot Reactants in a Plasmon-Assisted Chemical Reaction. *J. Am. Chem. Soc.* **2023**, *145* (22), 12264–12274. https://doi.org/10.1021/jacs.3c02681.
(13) Boerigter, C.; Campana, R.; Morabito, M.; Linic, S. Evidence and Implications of Direct Charge Excitation as the Dominant Mechanism in Plasmon-Mediated Photocatalysis. *Nat. Commun.* **2016**, *7* (1), 10545. https://doi.org/10.1038/ncomms10545.
(14) Kale, M. J.; Avanesian, T.; Christopher, P. Direct Photocatalysis by Plasmonic Nanostructures. *ACS Catal.* **2014**, *4* (1), 116–128. https://doi.org/10.1021/cs400993w.
(15) Shetty, M.; Walton, A.; Gathmann, S. R.; Ardagh, M. A.; Gopeesingh, J.; Resasco, J.; Birol, T.; Zhang, Q.; Tsapatsis, M.; Vlachos, D. G.; Christopher, P.; Frisbie, C. D.; Abdelrahman, O. A.; Dauenhauer, P. J. The Catalytic Mechanics of Dynamic Surfaces: Stimulating Methods for Promoting Catalytic Resonance. *ACS Catal.* **2020**, *10* (21), 12666–12695. https://doi.org/10.1021/acscatal.0c03336.
(16) Qi, J.; Resasco, J.; Robatjazi, H.; Alvarez, I. B.; Abdelrahman, O.; Dauenhauer, P.; Christopher, P. Dynamic Control of Elementary Step Energetics via Pulsed Illumination Enhances Photocatalysis on Metal Nanoparticles. *ACS Energy Lett.* **2020**, *5* (11), 3518–3525. https://doi.org/10.1021/acsenergylett.0c01978.
(17) Ardagh, M. A.; Abdelrahman, O. A.; Dauenhauer, P. J. Principles of Dynamic Heterogeneous Catalysis: Surface Resonance and Turnover Frequency Response. *ACS Catal.* **2019**, *9* (8), 6929–6937. https://doi.org/10.1021/acscatal.9b01606.
(18) Song, H.; Meng, X.; Dao, T. D.; Zhou, W.; Liu, H.; Shi, L.; Zhang, H.; Nagao, T.; Kako, T.; Ye, J. Light-Enhanced Carbon Dioxide Activation and Conversion by Effective Plasmonic Coupling Effect of Pt and Au Nanoparticles. *ACS Appl. Mater. Interfaces* **2018**, *10* (1), 408–416. https://doi.org/10.1021/acsami.7b13043.
(19) Song, H.; Meng, X.; Wang, Z.; Wang, Z.; Chen, H.; Weng, Y.; Ichihara, F.; Oshikiri, M.; Kako, T.; Ye, J. Visible-Light-Mediated Methane Activation for Steam Methane Reforming under Mild Conditions: A Case Study of Rh/TiO2 Catalysts. *ACS Catal.* **2018**, *8* (8), 7556–7565. https://doi.org/10.1021/acscatal.8b01787.
(20) Bian, X.; Zhao, Y.; Waterhouse, G. I. N.; Miao, Y.; Zhou, C.; Wu, L. Z.; Zhang, T. Quantifying the Contribution of Hot Electrons in Photothermal Catalysis: A Case Study of Ammonia Synthesis over Carbon-Supported Ru Catalyst. *Angew. Chem. - Int. Ed.* **2023**, *62* (25), 1–8. https://doi.org/10.1002/anie.202304452.
(21) Zhang, X.; Li, X.; Reish, M. E.; Zhang, D.; Su, N. Q.; Gutiérrez, Y.; Moreno, F.; Yang, W.; Everitt, H. O.; Liu, J. Plasmon-Enhanced Catalysis: Distinguishing Thermal and Nonthermal Effects. *Nano Lett.* **2018**, *18* (3), 1714–1723. https://doi.org/10.1021/acs.nanolett.7b04776.
(22) Sivan, Y.; Baraban, J.; Un, I. W.; Dubi, Y. Comment on "Quantifying Hot Carrier and Thermal Contributions in Plasmonic Photocatalysis." *Science* **2019**, *364* (6439), 87–93. https://doi.org/10.1126/science.aaw9367.
(23) Beck, A.; Marlowe, J.; Gordon, M. J.; Christopher, P. Is There a Discernible Photochemical Effect Beyond Heating for Visible Photon-Mediated NH3 Decomposition over Ru/Al2O3? *J. Phys. Chem. C* **2024**. https://doi.org/10.1021/acs.jpcc.4c00226.
(24) Budde, F.; Hamza, A. V.; Ferm, P. M.; Ertl, G.; Weide, D.; Andresen, P.; Freund, H.-J. Photodesorption of NO from Ni(100)-O. *Phys. Rev. Lett.* **1988**, *60* (15), 1518–1521.
(25) Hasselbrink, E.; Hirayama, H.; de Meijere, A.; Weik, F.; Wolf, M.; Ertl, G. Photodissociation and Photodesorption of O2 Adsorbed on Pd(111). *Surf. Sci.* **1992**, *269–270* (C), 235–246. https://doi.org/10.1016/0039-6028(92)91256-B.
(26) Hertel, T.; Wolf, M.; Ertl, G. Angular Distributions in Stimulated Desorption: Photodesorption of Ammonia from a Cu(111) Surface. *Chem. Phys. Lett.* **1996**, *257* (1–2), 155–162. https://doi.org/10.1016/0009-2614(96)00527-1.
(27) Ferm, P. M.; Budde, F.; Hamza, A. V.; Jakubith, S.; Ertl, G.; Weide, D.; Andresen, P.; Freund, H. J. UV-Laser-Induced Photodesorption of NO from NiO. *Surf. Sci.* **1989**, *218* (2–3), 467–493. https://doi.org/10.1016/0039-6028(89)90163-5.
(28) Hertel, T.; Wolf, M.; Ertl, G. UV Photostimulated Desorption of Ammonia from Cu(111). *J. Chem. Phys.* **1995**, *102* (8), 3414–3430. https://doi.org/10.1063/1.469215.

(29) Beck, A.; Paunović, V.; van Bokhoven, J. A. Identifying and Avoiding Dead Ends in the Characterization of Heterogeneous Catalysts at the Gas–Solid Interface. *Nat. Catal.* **2023**, *6* (10), 873–884. https://doi.org/10.1038/s41929-023-01027-x.
(30) Loh, J. Y. Y.; Wang, A.; Mohan, A.; Tountas, A. A.; Gouda, A. M.; Tavasoli, A.; Ozin, G. A. Leave No Photon Behind: Artificial Intelligence in Multiscale Physics of Photocatalyst and Photoreactor Design. *Adv. Sci.* **2024**, *2306604*, 1–15. https://doi.org/10.1002/advs.202306604.
(31) Barraza Alvarez, I.; Le, T.; Hosseini, H.; Samira, S.; Beck, A.; Marlowe, J.; Montemore, M. M.; Wang, B.; Christopher, P. Bond Selective Photochemistry at Metal Nanoparticle Surfaces: CO Desorption from Pt and Pd. *J. Am. Chem. Soc.* **2024**, *146* (18), 12431–12443. https://doi.org/10.1021/jacs.3c13874.
(32) Henglein, F. A. Formation of a Pt-Carbonyl Colloid by Reaction of Colloidal Pt with CO. *J. Phys. Chem. B* **1997**, *101* (31), 5889–5894. https://doi.org/10.1021/jp9710493.
(33) Chou, K. C.; Westerberg, S.; Shen, Y. R.; Ross, P. N.; Somorjai, G. A. Probing the Charge-Transfer State of CO on Pt(111) by Two-Dimensional Infrared-Visible Sum Frequency Generation Spectroscopy. *Phys. Rev. B* **2004**, *69* (15), 153413. https://doi.org/10.1103/PhysRevB.69.153413.
(34) Gorte, R. Design Parameters for Temperature Programmed Desorption from Porous Catalysts. *J. Catal.* **1982**, *75* (1), 164–174. https://doi.org/10.1016/0021-9517(82)90131-2.
(35) Kale, M. J.; Christopher, P. Utilizing Quantitative in Situ FTIR Spectroscopy To Identify Well-Coordinated Pt Atoms as the Active Site for CO Oxidation on Al 2 O 3 -Supported Pt Catalysts. *ACS Catal.* **2016**, *6* (8), 5599–5609. https://doi.org/10.1021/acscatal.6b01128.
(36) Kim, T. S.; O'Connor, C. R.; Reece, C. Interrogating Site Dependent Kinetics over SiO2-Supported Pt Nanoparticles. *Nat. Commun.* **2024**, *15* (1), 1–12. https://doi.org/10.1038/s41467-024-46496-1.
(37) Greenler, R. G.; Brandt, R. K. The Origins of Multiple Bands in the Infrared Spectra of Carbon Monoxide Adsorbed on Metal Surfaces. *Colloids Surf. Physicochem. Eng. Asp.* **1995**, *105* (1), 19–26. https://doi.org/10.1016/0927-7757(95)03336-X.
(38) Monai, M. A New Look at Catalyst Surfaces at Work: Introducing Mixed Isotope Operando Infrared Spectroscopy (MIOIRS). *ACS Catal.* **2025**, 1363–1386. https://doi.org/10.1021/acscatal.4c06308.
(39) Siddiqui, H. R.; Chen, P. J.; Guo, X.; Yates, J. T., Jr. A Comparative Kinetic Study of Xenon Adsorption on a Flat Pt(111) and Stepped Pt(557) and Pt(112) Surfaces. *J. Chem. Phys.* **1990**, *92* (12), 7690–7699. https://doi.org/10.1063/1.458155.
(40) Siddiqui, H. R.; Guo, X.; Chorkendorff, I.; Yates, J. T. CO Adsorption Site Exchange between Step and Terrace Sites on Pt(112). *Surf. Sci.* **1987**, *191* (1–2), L813–L818. https://doi.org/10.1016/S0039-6028(87)81043-9.
(41) Jbir, I.; Couble, J.; Khaddar-Zine, S.; Ksibi, Z.; Meunier, F.; Bianchi, D. Individual Heat of Adsorption of Adsorbed CO Species on Palladium and Pd-Sn Nanoparticles Supported on Al2O3 by Using Temperature-Programmed Adsorption Equilibrium Methods. *ACS Catal.* **2016**, *6* (4), 2545–2558. https://doi.org/10.1021/acscatal.5b02749.
(42) Campbell, C. T.; Ertl, G.; Kuipers, H.; Segner, J. A Molecular Beam Investigation of the Interactions of CO with a Pt(111) Surface. *Surf. Sci.* **1981**, *107* (1), 207–219. https://doi.org/10.1016/0039-6028(81)90621-X.
(43) Allian, A. D.; Takanabe, K.; Fujdala, K. L.; Hao, X.; Truex, T. J.; Cai, J.; Buda, C.; Neurock, M.; Iglesia, E. Chemisorption of CO and Mechanism of CO Oxidation on Supported Platinum Nanoclusters. *J. Am. Chem. Soc.* **2011**, *133* (12), 4498–4517. https://doi.org/10.1021/ja110073u.
(44) Heinz, K.; Barthel, A.; Hammer, L.; Müller, K. Kinetics of the Irreversible Transition Pt(110)1×1→1×2 as Observed by LEED. *Surf. Sci.* **1987**, *191* (1–2), 174–184. https://doi.org/10.1016/S0039-6028(87)81055-5.
(45) Perutz, R. N.; Procacci, B. Photochemistry of Transition Metal Hydrides. *Chem. Rev.* **2016**, *116* (15), 8506–8544. https://doi.org/10.1021/acs.chemrev.6b00204.
(46) J. Turner, J.; W. George, M.; Poliakoff, M.; N. Perutz, R. Photochemistry of Transition Metal Carbonyls. *Chem. Soc. Rev.* **2022**, *51* (13), 5300–5329. https://doi.org/10.1039/D1CS00826A.
(47) Avanesian, T.; Christopher, P. Adsorbate Specificity in Hot Electron Driven Photochemistry on Catalytic Metal Surfaces. *J. Phys. Chem. C* **2014**, *118* (48), 28017–28031. https://doi.org/10.1021/jp509555m.
(48) Olsen, T.; Gavnholt, J.; Schiøtz, J. Hot-Electron-Mediated Desorption Rates Calculated from Excited-State Potential Energy Surfaces. *Phys. Rev. B* **2009**, *79* (3), 035403. https://doi.org/10.1103/PhysRevB.79.035403.
(49) Menzel, D.; Gomer, R. Electron-Impact Desorption of Carbon Monoxide from Tungsten. *J. Chem. Phys.* **1964**, *41* (11), 3329–3351. https://doi.org/10.1063/1.1725731.
(50) Zhou, Y.; Doronkin, D. E.; Zhao, Z.; Plessow, P. N.; Jelic, J.; Detlefs, B.; Pruessmann, T.; Studt, F.; Grunwaldt, J. D. Photothermal Catalysis over Nonplasmonic Pt/TiO2 Studied by Operando HERFD-XANES, Resonant XES, and DRIFTS. *ACS Catal.* **2018**, *8* (12), 11398–11406. https://doi.org/10.1021/acscatal.8b03724.
(51) Psarellis, Y. M.; Kavousanakis, M. E.; Dauenhauer, P. J.; Kevrekidis, I. G. Writing the Programs of Programmable Catalysis. *ACS Catal.* **2023**, *13* (11), 7457–7471. https://doi.org/10.1021/acscatal.3c00864.
(52) Dauenhauer, P. J. Up up down down Left Right Left Right B A Start for the Catalytic Hackers of Programmable Materials. *Matter* **2023**, *6* (12), 4145–4157. https://doi.org/10.1016/j.matt.2023.11.008.

(53) Gravejat, P.; Derrouiche, S.; Farrussengn, D.; Lombaert, K.; Mirodatos, C.; Bianchi, D. Heats of Adsorption of Linear and Bridged CO Species Adsorbed on a 3% Ag/Al2O3 Catalyst Using in Situ FTIR Spectroscopy under Adsorption Equilibrium. *J. Phys. Chem. C* **2007**, *111* (26), 9496–9503. https://doi.org/10.1021/jp072055u.

Acknowledgments. A.B., M.G., and P.C. acknowledge support from the Center for Programmable Energy Catalysis, a U.S. Department of Energy (DOE) Energy Frontier Research Center (DE-SC0023464). We also acknowledge O. A. Abdelrahman and P. J Dauenhauer during the writing of the manuscript. Further, we thank I. Barraza Alvarez, R. Berry, S. Marino, S. Samira, O. Polonskyi, and N. Lim for the discussions on the experimental setup and data evaluation.

Competing interests. The authors declare no competing interests.